Noname manuscript No.
(will be inserted by the editor)

Gait Design and Experimental Validation of a Snake Robot on a Pipe with Branches Using Spiral Stairs Function

Mizuki Nakajima · Qi Cheng · Motoyasu Tanaka

Received: date / Accepted: date

Abstract This paper presents the gait design and experimental validation of a snake robot on a pipe with branches. The target posture of the robot is designed as a continuous curve, and the robot moves by changing the shape of the curve and the area that it approximates. Additionally, the paper presents a novel target shape for a snake robot when moving on a pipe with branches. In the proposed gait, the robot does not contact the pipe with its entire body, and a part of its body is lifted away from the pipe. The contact points between the robot and the pipe move freely using the shifting and rolling motions. The robot surpasses the branches of the pipe by switching the contact points between itself and the pipe. The effectiveness of the proposed gait was demonstrated by simulations using a physics simulator and experiments with an actual robot.

Keywords Snake robot · Pipe · Branch

1 Introduction

A snake robot comprises links and rotating joints and has several degrees of freedom (DOFs). It can move in various environments and perform diverse motions using its high DOF: moving on a slope based on CPG [1], traversing a terrain comprising multiple slopes, based on the sidewinding [2], climbing a ladder by changing the shape of the robot similar to a hook [3], semi-autonomous stair climbing by a snake robot with active wheels [4], etc. Inspection of the insides and outsides of pipes is also expected to be one of the applications of the snake robot.

The helical rolling motion facilitates the robot's movement on the outside of the pipe [5]. In this method, the robot changes its body shape into a spiral, wraps itself around the pipe by the body, and moves on the outside of the pipe by twisting its body. However, this method is not directly applicable to pipes with branches or obstacles because the robot moves in a direction perpendicular to the length of the body.

In [6], Takemori et al. represented complex shapes by connecting simple shapes and realized movement on pipes while avoiding flanges. Qi et al. proposed the helical wave propagation motion in [7] for a pipe with branches. In this method, the robot can move along the direction of the body length by superimposing a propagation wave on a spiral shape. This method enables the snake robot to move on the outside of the pipe while avoiding branches. However, the travel speed along the length of the body is much smaller than that of the rolling motion.

This paper presents a novel gait of a snake robot using a spiral stair function to improve the robot's moving speed on the outside of a pipe with branches. In the proposed gait, the robot does not contact the pipe with its entire body, and part of its body is lifted away from the pipe. The contact points between the robot and the pipe move freely using the shifting and rolling motion, and the robot can surpass the branches on the pipe. The effectiveness of the proposed gait was demonstrated through simulations and experiments with an actual robot.

This work was presented in part at the 4th International Symposium on Swarm Behavior and Bio-Inspired Robotics, Online, June 1-4, 2021.

Mizuki Nakajima
The University of Electro-Communications, 1 5 1 Chofugaoka, Chofu, Tokyo, Japan
E-mail: mizuki.nakajima@rc.mce.uec.ac.jp

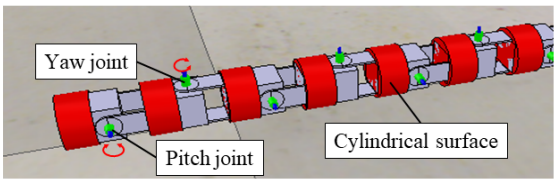

Fig. 1 Model of a snake robot

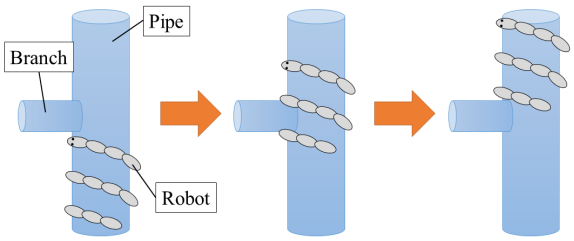

Fig. 2 A pipe and branch

2 Problem settings

Fig. 1 depicts the structure of the snake robot. The robot's links are connected in series by rotational joints. The odd- and even-numbered joints are the pitch and yaw rotational joints, respectively. The exterior of the robot is smooth and cylindrical, as shown in Fig. 1. The friction coefficient of the robot's exterior is assumed to be high, and the contact between the environment and the robot generates a high frictional force. Each joint has a limited range of motion owing to interference with adjacent links.

Fig. 2 depicts the assumed environment and the robot's movement on the outside of the pipe. A pipe with a right-angle bent branch was assumed, and excessively small and large branches were not considered. The purpose of the motion is to allow the robot to move on the outside of the pipe while avoiding the branches. In the previous method of [7], the robot moved using the motion of helical wave propagation while surpassing the branches. The moving speed of the helical wave propagation is significantly lower than that of the rolling motion. Therefore, the moving speed is significantly reduced when the robot surpasses the branches.

3 Gait design using spiral stair function

The robot has several links and joints, and the computational cost of the motion design based on a discrete link model for the robot is high. To reduce the computational cost, a control method in which the target posture of the robot is designed as a continuous curve, similar to that in [9], is often used. Similar to that in [9], the target posture of the robot is designed as a continuous curve, and the joint angle of the robot is calculated by fitting the robot's body into a continuous curve.

3.1 Calculation of the joint angle

The robot's body shape is represented by a continuous curve, as shown in Fig. 3. By using the Frenet-Serret formula, the curve can be described as

$$\begin{cases} \dfrac{d\boldsymbol{c}(s)}{ds} &= \boldsymbol{e}_1(s) \\ \dfrac{d\boldsymbol{e}_1(s)}{ds} &= \kappa(s)\boldsymbol{e}_2(s) \\ \dfrac{d\boldsymbol{e}_2(s)}{ds} &= -\kappa(s)\boldsymbol{e}_1(s) + \tau(s)\boldsymbol{e}_3(s) \\ \dfrac{d\boldsymbol{e}_3(s)}{ds} &= -\tau(s)\boldsymbol{e}_2(s) \end{cases} \tag{1}$$

where s is the length of the curve from the starting point, $\kappa(s)$ is the curvature, $\tau(s)$ is the torsion, and $\boldsymbol{c}(s) = [x(s),\ y(s),\ z(s)]^{\mathrm{T}}$ is a vector representing the curve. Furthermore, $\boldsymbol{e}_1(s)$, $\boldsymbol{e}_2(s)$, and $\boldsymbol{e}_3(s)$ are defined as in Fig. 3.

Additionally, for an actual snake robot, the orientation of the robot's back and belly must also be considered. A representation using backbone curves is proposed in [10]. Fig. 3 presents a backbone coordinate system, $\boldsymbol{e}_{\mathrm{r}}(s)$, $\boldsymbol{e}_{\mathrm{p}}(s)$, $\boldsymbol{e}_{\mathrm{y}}(s)$. The backbone curve is represented as

$$\begin{cases} \dfrac{d\boldsymbol{c}(s)}{ds} &= \boldsymbol{e}_{\mathrm{r}}(s) \\ \dfrac{d\boldsymbol{e}_{\mathrm{r}}(s)}{ds} &= \kappa_{\mathrm{y}}(s)\boldsymbol{e}_{\mathrm{p}}(s) - \kappa_{\mathrm{p}}(s)\boldsymbol{e}_{\mathrm{y}}(s) \\ \dfrac{d\boldsymbol{e}_{\mathrm{p}}(s)}{ds} &= -\kappa_{\mathrm{y}}(s)\boldsymbol{e}_{\mathrm{r}}(s) \\ \dfrac{d\boldsymbol{e}_{\mathrm{y}}(s)}{ds} &= \kappa_{\mathrm{p}}(s)\boldsymbol{e}_{\mathrm{r}}(s) \end{cases} \tag{2}$$

where κ_{p} and κ_{y} are the curvatures around the pitch and yaw joints, respectively.

The parameters of the Frenet-Serret formula (1) can be converted to those of the backbone curve (2) using the following equations:

$$\begin{cases} \kappa_{\mathrm{p}}(s) = -\kappa(s)\sin(\psi(s)) \\ \kappa_{\mathrm{y}}(s) = \kappa(s)\cos(\psi(s)) \\ \psi(s) = \displaystyle\int_0^s \tau ds + \psi(0) \end{cases} \tag{3}$$

where $\psi(0)$ is an integral constant that represents the initial value of torsion, and can be freely designed. If $\psi(0)$ changes, the backbone coordinate of the robot rotates around the curve and the rolling motion can be realized.

s_{h} denotes the s of the robot head. The position of the robot in the continuous curve can be shifted by changing s_{h}. Then, the following equation can be used

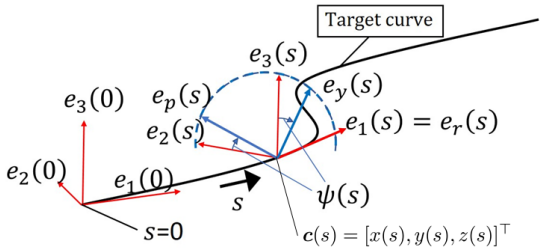

Fig. 3 Continuous curve and parameters

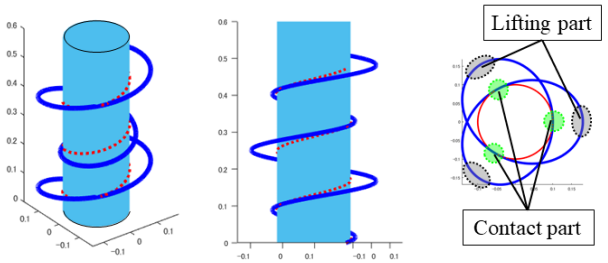

(a) Perspective view (b) Side view (c) Top view

Fig. 4 Proposed curve

to approximate the i-joint angle, ρ_i, of the robot as follows [9]:

$$\rho_i = \begin{cases} \int_{s_h+(i-1)l_k}^{s_h+(i+1)l_k} \kappa_p ds & (i : odd) \\ \int_{s_h+(i-1)l_k}^{s_h+(i+1)l_k} \kappa_y ds & (i : even) \end{cases} \tag{4}$$

3.2 Target continuous curve

In the gait design with continuous curves, the robot moves via two motions. One is the shifting motion that shifts the body shape along the curve, and the other is the rolling motion that rotates the entire body around the curve. For the helical rolling motion, the target curve is designed such that the entire body of the robot is in contact with the pipe. In contrast, in the proposed motion, a body part that does not make contact with the pipe has been introduced intentionally. By introducing a body part that is not in contact with the environment, various motions can be generated by moving the contact point. Introducing the lifting part and changing the contact point have been used in various situations, such as moving on the outside of the pipe [6, 7], sidewinding [11] and sinus-lifting [12] like a real snake, obstacle avoidance using redundancy [13], and steering a handcart using the head and tail [15].

This paper proposes a novel curve with a point that does not contact the pipe, as shown in Fig. 4. By combining the shifting and rolling motions, the robot can move in an arbitrary direction in the pipe. The novel curve is represented as

$$\begin{cases} x = (R - r)\sin(\theta + \theta_0) - R\sin(K\theta + \theta_0) \\ y = (R - r)\cos(\theta + \theta_0) + R\cos(K\theta + \theta_0) \\ z = k\theta \end{cases} \tag{5}$$

where R is the maximum length between the central axis of the pipe and the curve, r is the radius of the pipe, θ is the intervening variable, θ_0 is the initial phase angle related to θ, K is the frequency of the curve, and k is a parameter related to the height of the curve. Considering its shape, the curve is termed as *spiral stairs function* in this study. By using the proposed curve, the robot makes a contact with the pipe only through a specific part (contact part in Fig. 4). The contact points between the robot and the pipe pass through a helix, denoted by $z = k\theta/K$. This helix is called the *contact helix*. It should be noted that the path of movement of the contact point owing to rolling or shifting does not pass through the contact helix, but only the contact point in the stationary state is placed on the helix. The contact point moves in different directions between the shifting and rolling motions, as shown in Fig. 5. Therefore, by combining the two motions, the contact point can be moved in an arbitrary direction. If the movement of the contact point is properly designed, the robot can pass a branch on the pipe. The sizes of the pipes and branches that can be passed using the proposed method change depending on the parameters of the curve. Theoretically, it is possible to adapt to an arbitrary pipe by changing the parameters; however, in real-world robots, the adaptable environment is limited by factors such as the movement limits of the joints, joint torque, and length of the robot. The theoretical limits of the adaptable environment have not been derived. Consideration of the constraints on the adaptive environment is a subject of future research.

Let δs and $\delta\theta$ be the small changes in s and θ, respectively. The relationship between δs and $\delta\theta$ is obtained by

$$\delta s = \delta\theta \sqrt{\left(\frac{dx}{d\theta}\right)^2 + \left(\frac{dy}{d\theta}\right)^2 + \left(\frac{dz}{d\theta}\right)^2}. \tag{6}$$

The torsion τ and curvature κ of the continuous curve is obtained by

$$\tau = \frac{x'''(y'z''-z'y'')+y'''(z'x''-x'z'')+z'''(x'y''-y'x'')}{(y'z''-z'y'')^2+(z'x''-x'z'')^2+(x'y''-y'x'')^2} \tag{7}$$

$$\kappa = \frac{\sqrt{(y'z''-z'y'')^2+(z'x''-x'z'')^2+(x'y''-y'x'')^2}}{(x'^2+y'^2+z'^2)^{\frac{3}{2}}} \tag{8}$$

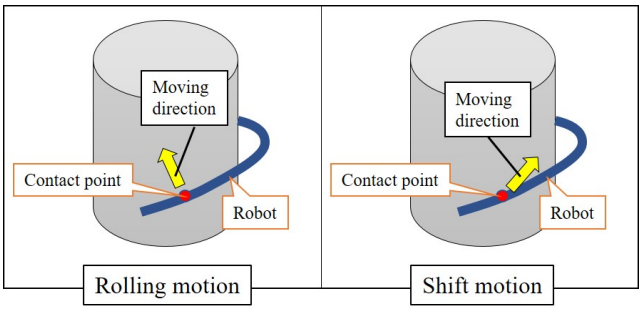

Fig. 5 Motion of a contact point between the robot and pipe

where $' = \frac{d}{ds}, '' = \frac{d^2}{ds^2}, ''' = \frac{d^3}{ds^3}$. By integrating (6) numerically, the value of θ corresponding to s can be obtained. Furthermore, τ and κ are obtained by substituting θ into (7) and (8). Finally, the relative joint angle, ρ_i, is obtained by substituting τ and κ into (3) and (4).

3.3 Moving path of the proposed gait

This section provides a detailed discussion of the movement path of the proposed gait. As aforementioned, the contact point between the robot and the pipe is located on the contact helix; however, the inclination of the robot at the contact point is different from that of the contact helix. Therefore, the movement path in the rolling and shifting motion is different from that of the helical wave propagation motion [7] and helical rolling motion [5] in previous studies.

First, the movement path of the shifting motion is discussed. Assuming that the contact part between the robot and the pipe does not slip, the contact point moves smoothly over the pipe via the shifting motion. In this case, the path is like rolling a cylinder on the pipe, as shown in Fig. 6(a). The path of the contact point when the cylinder is rolled on the pipe is close to the path of the contact point of the shifting motion, as shown in Fig. 6(a). Fig. 6(b) shows the movement path of the shifting motion. Let S' be the surface which is orthogonal to the x-y plane and passes through the target body shape. When S' is wrapped around the pipe, the path of the contact point is derived from the target body shape. The moving path of the contact point cannot be obtained analytically because the calculation process includes integration in the length direction of the curve. From the geometric relationship, the inclination of the path of the contact point is smaller than that of the contact helix. It should be noted that this path is only the movement path of the contact point, and the position of the contact point in the body changes. This shows that certain parts of the robot's body, such as the robot's tail, do not follow this path.

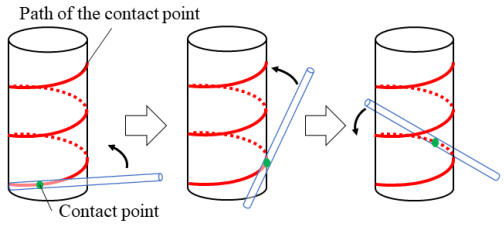

(a) Overview of the path

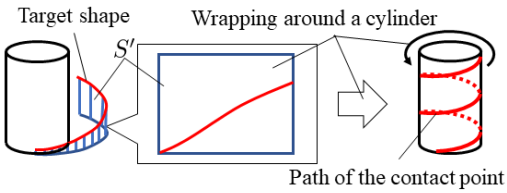

(b) Procedure of the calculation of the path

Fig. 6 Path of the contact point in the shift motion

Second, the path of the rolling motion is discussed. In the rolling motion, the contact point moves in a direction orthogonal to the trunk axis. Fig. 7 depicts the movement path of the rolling motion. It should be noted that the rolling motion rotates the entire robot in the direction opposite to that of the shifting motion. The inclination of the robot at the contact point is more gradual than that of the contact helix. Moreover, the z-axis travel is larger, and the rotation around the pipe is smaller than that of the normal helix rolling motion.

In the proposed gait, the contact point between the pipe and the robot can be controlled using rolling and shifting motions simultaneously. For example, while avoiding an obstacle such as a branch on a pipe, the contact point is controlled to move on the contact helix, as shown in Fig. 8, to avoid the obstacle. In actual, the joint angular velocity, joint torque, and length of the robot cause constraints on the parameters and selectable paths. The joint angular velocity affects the limiting speed of the rolling and shifting, whereas the joint torque and total length affect the adaptable pipe radius.

4 Comparison with previous study

This section provides a comparison with the previous study, [7]. To surpass an obstacle such as a branch pipe on the pipe while the body of the robot is wrapped around the pipe, the entire robot must rotate around the pipe. Then, the amount of rotation around the pipe

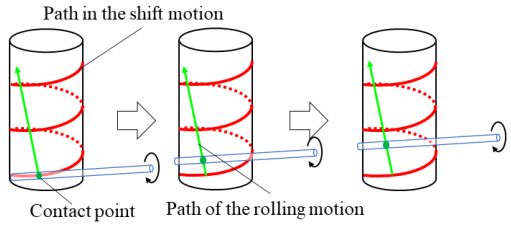

Fig. 7 Path of the contact point in the rolling motion

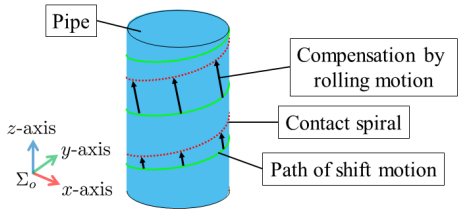

Fig. 8 Compensation of the path by the rolling motion

for the helical wave propagation motion [7] and the proposed motion are compared. To avoid obstacles with the proposed motion, an appropriate rolling motion is required in addition to the shifting motion. Therefore, in this comparison, the amount of rotation around the pipe when the shifting and rolling motions are combined and controlled such that the contact point passes over the contact helix is compared with the previous study.

In the previous study, the robot moved along a helix by approximating the body shape to the target curve. The target curve has the shape of a small wave superimposed on the reference helix. The target body shape is represented by the following equations with the mediator θ.

$$\begin{cases} x = a\cos(\theta) \\ y = a\sin(\theta) \\ z = b\theta \end{cases} \tag{9}$$

where,

$$a = r_{hwp} + A\mathrm{sech}(w\theta - \phi) \tag{10}$$

where A is the height of the sending wave, w is the width of the wave, ϕ is the position of the wave on the curve, r_{hwp} is the radius of the reference helix, and b is the parameter that determines the slope of the helix. By changing ϕ, the curve changes similar to that when sending a wave on the helix. The robot moves along the curve by changing its body shape to match the curve. Changing ϕ corresponds to the shifting motion in the proposed gait. The amount of movement cannot be determined analytically for both the previous and proposed gaits. Therefore, the amount of rotation around the pipe, Θ, under several conditions was

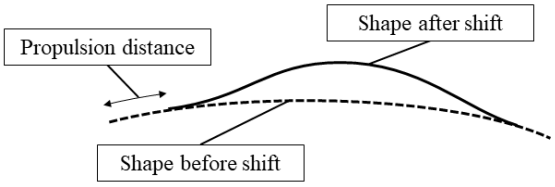

Fig. 9 Path of the helical wave propagation

Table 1 Rotation around a pipe

	Previous method			Proposed method		
	(i)	(ii)	(iii)	(i)	(ii)	(iii)
Θ [rad]	1.53	0.785	0.419	4.87	4.93	4.92

numerically calculated. The value of Θ was obtained from the position of the robot's tail. For the parameters of each method, $b = k/K$ and $A = 2R - r$ were introduced to make the conditions as close as possible. These equations were set such that the distance between the farthest point of the target curve from the pipe and the central axis of the pipe in each method are equal, and the slope of the contact helix in the proposed method and the reference helix in the previous method are equal.

The common parameters for each condition in the previous method are the pipe radius $r_p = 0.10$ m, robot link radius $r_b = 0.02$ m, radius of the reference helix in the target curve $r_{hwp} = 0.12$, wave height $A = 0.03$ m. Furthermore, the parameters that determine the slope of the reference helix in the previous method are $b = 0.025$ m/rad, $\theta_0 = -\pi/2$ rad, and $R = 0.135$ m. Regarding the parameters to be varied, $w = 0.5, 1.0, 2.0$ are conditions (i)–(iii) of the conventional method and $K = 2, 4, 8$ are the conditions (i)–(iii) of the proposed method, respectively. Additionally, k was set to $k = Kb$ using the above equation. The amount of the shift was $s = 2.0$. The simulation results for each condition are listed in Table 1. From Table 1, it is evident that the proposed motion has more rotation around the pipe than that in the conventional study. Therefore, the proposed motion can pass over the branch on the pipe more quickly than the conventional method.

5 Simulations

Simulations were conducted to demonstrate the effectiveness of the proposed gait. For the simulation, the physics simulator V-rep [16] (COPPELIA ROBOTICS Inc.) was used, and the Bullet was used as the physics calculation engine. Fig. 10 shows the simulation model. The number of joints is 33, and the length, diameter,

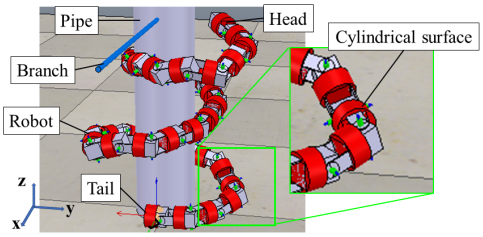

Fig. 10 Simulation model

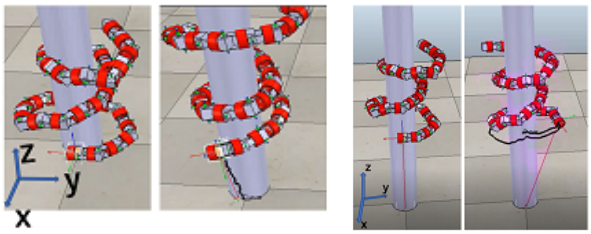

(a) Rolling motion (b) Shift motion

Fig. 11 Simulation result ($g = 0$ m/s^2)

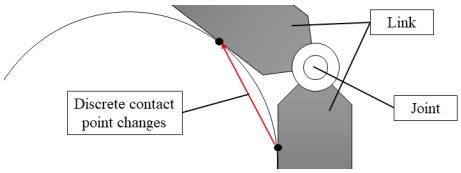

Fig. 12 Discrete changes of the contact point

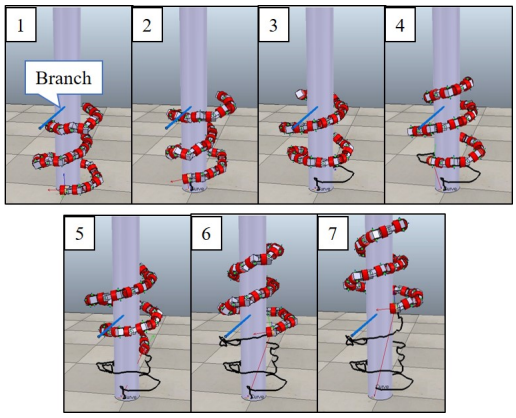

Fig. 13 Pass through the branch on the pipe ($g = 0$ m/s^2)

and weight of the link are 0.07 m, 0.027 m, and 0.1 kg, respectively. The radius of the pipe is 0.073 m, and the frictional coefficient was 0.5. The frictional coefficient is an important parameter to ensure that the robot does not slip. If the frictional coefficient is low, the tightening force must be increased to increase the frictional force to prevent slipping.

5.1 Simulations without gravity ($g = 0$ m/s^2)

To eliminate the effect of sliding due to gravity, simulations were performed with gravitational acceleration g set to zero. The parameter values of R, r, and k were 0.15, 0.1, and 0.05 m, respectively, and $Kand\theta_0$ were 1.67 and 0, respectively. Fig. 11(a) shows the result of the rolling motion on a pipe with no branches. The black line represents the path of the robot's tail. As seen in Fig. 11(a), it was confirmed that the robot could climb the pipe via the rolling motion. Fig. 11(b) depicts the result of the shifting motion on the pipe with no branches. As seen in Fig. 11(b), the robot rotated around the pipe and moved only slightly in the z direction. Therefore, the rolling motion is required to move in the z direction. The direction of movement for both rolling and shifting motions tended to be close to their theoretical values. However, especially in the shift operation, the amount of rotation around the pipe was smaller than the theoretical value. This can be largely attributed to the fact that the simulation model comprises discrete links, whereas the theoretical values are derived from a continuum model. In the calculation of the theoretical values, the contact position between the robot and the pipe is assumed to change smoothly, whereas in the discrete link model, this contact position changes discretely, as shown in Fig. 12. In the event of such a discrete change in contact position, the amount of propulsion by the shifting motion is smaller than in the case of a smooth change. Consequently, the amount of rotation around the pipe was considered to be less than the theoretical value. However, the amount of rotation is still larger than that of the helical wave propagation motion [7], and the robot can be expected to surpass the branch pipe quickly. Additionally, the operator directly instructs the number of operations for the rolling and shifting motions. Therefore, the operation is not problematic unless the tendencies of the motions are significantly different. The autonomous operation of the robot and estimation of the actual amount of movement are subjects of future research.

Fig. 13 depicts the result of the experiment when the operator directly instructed the shifting and rolling motions. It was assumed that the position of the branch on the pipe was visible to the operator. The operator checked the relative positions of the robot and pipe and adjusted the amount of the rolling and shifting motions. With the adjustments in motions by the operator, the robot was able to pass the branch.

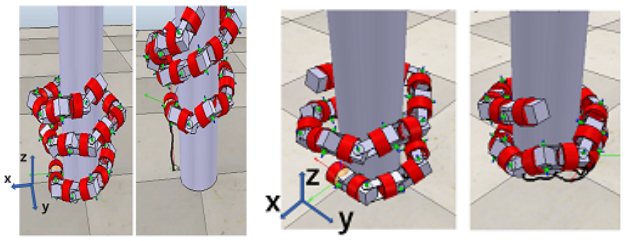

(a) Rolling motion (b) Shift motion

Fig. 14 Simulation results after changing parameters

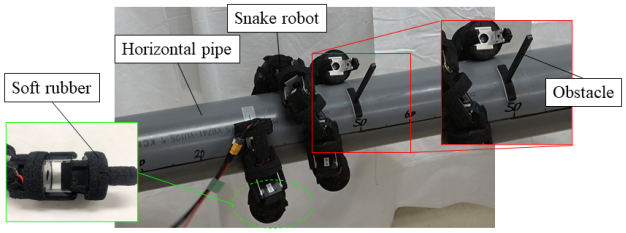

Fig. 15 Experimental environment and the robot

5.2 Simulations with gravity ($g = 9.8$ m/s^2)

To verify the behavior of the robot under the influence of gravity, simulations were conducted in an environment where the gravitational acceleration was $g = 9.8\text{m/s}^2$.

When a curve identical to that in the previous subsection was used in the simulation, the robot's body shape significantly deviated from the target shape owing to the effect of gravity, and the robot could not move on the pipe. Therefore, the simulation was performed by changing parameters R and k of the curve to 0.12 and 0.03, respectively. The results of the shifting and rolling motions are depicted in Figs. 14(a) and 14(b), respectively. The robot climbed the pipe via the rolling motion and rotated around the pipe via the shifting motion, as shown in Figs. 14(a) and 14(b), respectively. Eventually, it was confirmed that the proposed gait is feasible even in an environment with the influence of gravity.

6 Experiment

Experiments using an actual robot were performed to verify the effectiveness of the proposed gait. Fig. 15 depicts the actual robot and the experimental environment. The external shape of the robot is designed as a cylinder, and soft rubber is attached to the surface of the robot to generate a large frictional force when it contacts the pipe. The Dynamixel XH430-V350-R (ROBOTIS Inc.) motor was used to connect each link, and the joint angle could be controlled directly from the computer via serial communication. Each joint has a built-in angle sensor and current sensor, and the joint can be controlled by specifying the target angle. The number of joints was 20, and the length, diameter, and weight of the link were 0.07 m, 0.027 m, and 0.145 kg, respectively. The diameter of the pipe which was placed horizontally was 140 mm. An obstacle was placed on the pipe to simulate a branch, as shown in Fig. 15. The position of the obstacle on the pipe was assumed to be visible to the operator, and the operator adjusted the amount of the rolling and shifting movements based on the relative relationship between the obstacle and the robot.

First, the behavior of the shifting and rolling motions on a horizontal pipe with no branches was examined. Fig. 16 depicts each motion. As seen in Fig. 16(a), it was confirmed that the robot moved in the direction of the pipe axis via the rolling motion. In the shifting motion, the entire robot rotates around the pipe, as shown in Fig. 16(b). Next, the operator manually switched between the shifting and rolling motions to position the robot over a branch on the pipe. Fig. 17 presents the experimental result. The combination of shifting and rolling motions allowed the robot to traverse the branch on the pipe, as shown in Fig. 17. In conclusion, it was confirmed that with the proposed gait the robot could pass a branch on a horizontal pipe.

In contrast, when the pipe was placed vertically, the robot fell off the pipe and could not move on it. This behavior can be attributed to the lack of frictional force between the pipe and the robot, which is caused because the robot was lifted from the pipe owing to the approximation error to the target continuous curve or insufficient joint torque of the actual robot. In the simulation, a large joint torque can be output, and the pipes can be tightened very strongly. Consequently, a large frictional force was generated between the robot and the pipe. The propulsion was possible on the vertical pipe in the simulation. Therefore, it is expected that propulsion on a vertical pipe can be realized by an actual robot if the joint torque of the robot is sufficiently large. The improvement of the actual robot to realize the propulsion of a vertical pipe is a subject of future research.

7 Conclusion

This paper proposed a novel gait of a snake robot using a spiral stairs function for movement on a pipe with

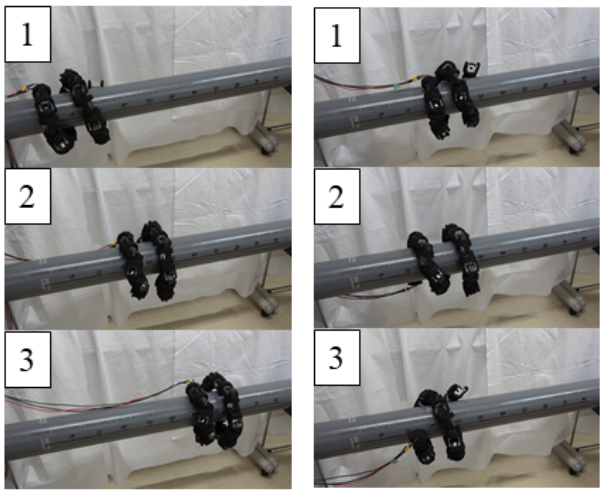

(a) Rolling motion (b) Shift motion

Fig. 16 Experimental result

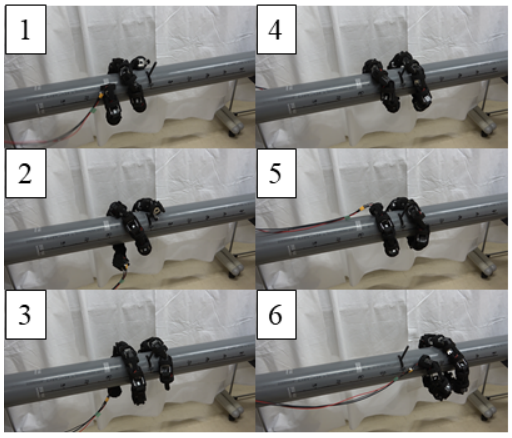

Fig. 17 Pass through the branch on the horizontal pipe

branches. The effectiveness of the proposed gait was demonstrated through simulations and experiments using an actual robot. Experiments demonstrated successful movement on a horizontal pipe; however, movement on a vertical pipe could not be realized owing to insufficient frictional force. Our future work will focus on the movement on a vertical pipe with an actual robot, autonomization, and improvement of the gait for a curved pipe.

References

1. Crespi A, Ijspeert AJ (2008) Online optimization of swimming and crawling in an amphibious snake robot. IEEE Transactions on Robotics 24(1):75-87. doi:10.1109/TRO.2008.915426
2. Gong C, Tesch M, Rollinson D, Choset H (2013) Snakes on an Inclined Plane: Learning an adaptive sidewinding motion for changing slopes. In: IEEE International Conference on Intelligent Robots and Systems, Chicago, IL, USA, Sept 2013, pp 1114-1119. doi:10.1109/IROS.2014.6942697
3. Takemori T, Tanaka M, Matsuno F (2018) Ladder Climbing with a Snake Robot. In: IEEE/RSJ International Conference on Intelligent Robots and Systems, Madrid, Spain, Oct 2018, pp 1-9. doi:10.1109/IROS.2018.8594411
4. Tanaka M, Nakajima M, Suzuki Y, Tanaka K (2018) Development and Control of Articulated Mobile Robot for Climbing Steep Stairs. IEEE/ASME Transactions on Mechatronics 23(2):531-541. doi:10.1109/TMECH.2018.2792013
5. Hatton R, et al (2010) Generating gaits for snake robots: annealed chain fitting and keyframe wave extraction. Autonomous Robots 28:271-281. doi:10.1007/s10514-009-9175-2
6. Takemori T, Tanaka M, Matsuno F (2018) Gait Design and Experiment for a Snake Robot Designed by Connecting Curve Segments. IEEE Transactions on Robotics 34(5):1384-1391. doi:10.1109/TRO.2018.2830346
7. Qi W, Kamegawa T, Gofuku A (2016) Proposal of helical wave propagate motion for a snake robot to across a branch on a pipe. In: IEEE/SICE International Symposium on System Integration, Sapporo, Japan, Dec 2016, pp 821-826. doi:10.1109/SII.2016.7844101
8. Qi W, Kamegawa T, Gofuku A (2019) Implementation of Helical Wave Propagation Motion in Snake Robot Moving on Exterior of a Pipe. International Journal of Advanced Mechatronic Systems 7(6):359-367. doi:10.1504/IJAMECHS.2017.099314
9. Yamada H, et al (2006) Study on the 3D shape of active cord mechanism. In: IEEE International Conference on Robotics and Automation, Orlando, FL, USA, May 2006, 2890-2895. doi:10.1109/ROBOT.2006.1642140
10. Yamada H, Hirose S (2008) Study of Active Cord Mechanism –Approximations to Continuous Curves of a Multi-joint Body–. Journal of the Robotics Society of Japan 26(1):110-120. doi:10.7210/jrsj.26.110. (in Japanese with English Summary)
11. Burdick JW, Radford J, Chirikjian GS (1994) A 'sidewinding' locomotion gait for hyper-redundant robots. Advanced Robotics 9(3):195-216. doi:10.1109/ROBOT.1993.291864
12. Toyoshima S, Tanaka M, Matsuno F (2014) A Study on Sinus-lifting Motion of a Snake Robot with Sequential Optimization of a Hybrid System. IEEE Transactions on Automation Science and Engineering 11(1):139-143. doi:10.1109/TASE.2013.2273356
13. Tanaka M, Kon K, Tanaka K (2015) Range-sensor-based Semiautonomous Whole-body Collision Avoidance of a Snake Robot. IEEE Transactions on Control Systems Technology 23(5):1927-1934. doi:10.1109/TCST.2014.2382578
14. Tanaka M, Tanaka K (2015) Control of a Snake Robot for Ascending and Descending Steps. IEEE Transactions on Robotics 31(2):511-520. doi:10.1109/TRO.2015.2400655
15. Nakajima M, Tanaka M, Tanaka K (2020) Simultaneous Control of Two Points for Snake Robot and Its Application to Transportation. IEEE Robotics and Automation Letters 5(1):111-118. doi:10.1109/LRA.2019.2947003
16. Rohmer E, et al (2013) V-REP: a Versatile and Scalable Robot Simulation Framework. In: IEEE/RSJ International Conference on Intelligent Robots and Systems, Tokyo, Japan, Nov 2013, pp 1321-1326. doi:10.1109/IROS.2013.6696520